Journal of
Applied
Crystallography

ISSN 0021-8898Received 6 June 2008
Accepted 26 September 2008

Scatterless hybrid metal–single-crystal slit for small-angle X-ray scattering and high-resolution X-ray diffraction

Youli Li,[a]* Roy Beck,[b] Tuo Huang,[c] Myung Chul Choi[b] and Morito Divinagracia[a]

[a]Materials Research Laboratory, University of California at Santa Barbara, Santa Barbara, CA 93106, USA, [b]Materials and Physics Departments, University of California at Santa Barbara, Santa Barbara, CA 93106, USA, and [c]Grinnell College, Grinnell, IA 50112-1690, USA. Correspondence e-mail: youli@mrl.ucsb.edu

A simple hybrid design has been developed to produce practically scatterless aperture slits for small-angle X-ray scattering and high-resolution X-ray diffraction. The hybrid slit consists of a rectangular single-crystal substrate (*e.g.* Si or Ge) bonded to a high-density metal base with a large taper angle ($> 10^\circ$). The beam-defining single-crystal tip is oriented far from any Bragg peak position with respect to the incident beam and hence produces none of the slit scattering commonly associated with conventional metal slits. It has been demonstrated that the incorporation of the scatterless slits leads to a much simplified design in small-angle X-ray scattering instruments employing only one or two apertures, with dramatically increased intensity (a threefold increase observed in the test setup) and improved low-angle resolution.

© 2008 International Union of Crystallography
Printed in Singapore – all rights reserved

1. Introduction

Apertures (pinholes and slits) are used ubiquitously in X-ray diffraction (XRD) instruments to define and collimate the beam, controlling beam size and divergence which are the two key parameters in setting the measurement resolution. Typical X-ray apertures are made from machined high-density metals (*e.g.* tungsten or tantalum) because of their high X-ray attenuation. However, the intrinsic nano- and microscale porosity of the polycrystalline metal materials, consisting of multiple grains and grain boundaries, as well as the roughness of the aperture edge, give rise to what is commonly referred to as parasitic or slit scattering (Gehrke *et al.*, 1995; Sinha *et al.*, 1988), which broadens the beam profile and increases background intensity, with detrimental effects on data quality. The most intense slit scattering generally occurs in the low-angle region, thus becoming the main limiting factor of resolution [$q_{\min}$, which is determined by the lowest scattering angle that can be measured; $q = 4\pi\sin(\theta)/\lambda$] in small-angle X-ray scattering (SAXS) instrumentation (Pedersen, 1993). Reducing parasitic scattering is one of the most important considerations in SAXS instrumentation design, especially for weakly scattering materials (Zemb *et al.*, 2003; Bösecke & Diat, 1997).

Conceptually, it is not difficult to realize that the use of single-crystal materials (*e.g.* Si or Ge) to fabricate X-ray aperture slits could lead to a dramatic reduction or even complete elimination of parasitic scattering, as theoretically there should be negligible scattering if the near-perfect crystal is positioned far from any Bragg peak. Indeed, Si-based single-crystal slits have been used at various synchrotron facilities to reduce slit scattering (*e.g.* Gehrke *et al.*, 1995). However, previous experiments have shown that surface scattering with Si-based slits may still generate extraneous slit scattering, which can be alleviated by tilting the slit edge with respect to the incident beam.

Here, we present a simple hybrid metal–single-crystal slit design with a large built-in tilt angle that can practically eliminate parasitic scattering from slits. The hybrid slit consists of a rectangular single-crystal substrate bonded to a high-density metal base with a large tapering angle away from the beam. In contrast to earlier work in which the Si slits were tilted only slightly from the beam, we have demonstrated that by using a large built-in tapering (tilt) angle (typically $> 10^\circ$, much larger than the beam divergence), we avoid any possibility of grazing incidence and thus are able to inhibit completely surface scattering from the slits. Experiments were conducted to investigate systematically parasitic slit scattering from both hybrid and conventional metallic slits. The results confirmed that a single-crystal Si-tipped slit produces no observable slit scattering at all on a laboratory SAXS setup. It was demonstrated that the incorporation of the scatterless slits led to a much simplified optical design for SAXS instrumentation (only one slit is required in most cases, compared with typically three in the conventional configuration), without any need for guard slits, with dramatically increased intensity (a threefold increase was observed in the test setup) and with improved low-angle resolution. Because of its simplicity, this scatterless design can be easily implemented on existing SAXS instruments with metallic slits to yield significant performance enhancement with minimal cost.

2. Hybrid slit design

Fig. 1(*a*) schematically shows the simple design of the hybrid slit and how it was used in the experiments. The beam-defining slit edge is made of a rectangular single-side polished (100) Si substrate (2.5 × 30 × 0.5 mm, long edge along [110]), which was bonded with a thin layer of glue to the tapered end of a metal base (brass or tungsten, thickness = 2 mm). The hybrid design offers several advantages over a monolithic single-crystal design. Most importantly, it allows variation of both the width and the pitch (tapering angle) of the Si edge, two parameters crucial to optimal performance, with relative ease. Additionally, it overcomes the technical difficulty and cost associated with making monolithic single-crystal slits. Furthermore, it minimizes detrimental X-ray transmission through the slit body owing to the use of a high-density metal base, which can be made from low-cost material as well.

The design also takes into account secondary effects which may contribute to background scattering. The width of the Si substrate is selected such that it protrudes above the metal base on the incident side, to block off completely the downstream propagation of any scattering from the metal base. The Si slit itself is oriented with respect to the incident beam in such a way that no Bragg reflections can occur, hence inhibiting slit scattering. In this geometry, the only scattering that contributes to the background will be from thermal diffuse scattering or phonon scattering and possibly X-ray fluorescence, all of which are intrinsically weak. However, as shown in Fig. 1(*a*), the tapered design exposes only a small part of the Si (above the tip of the metal base) to the beam, thus minimizing these parasitic effects.

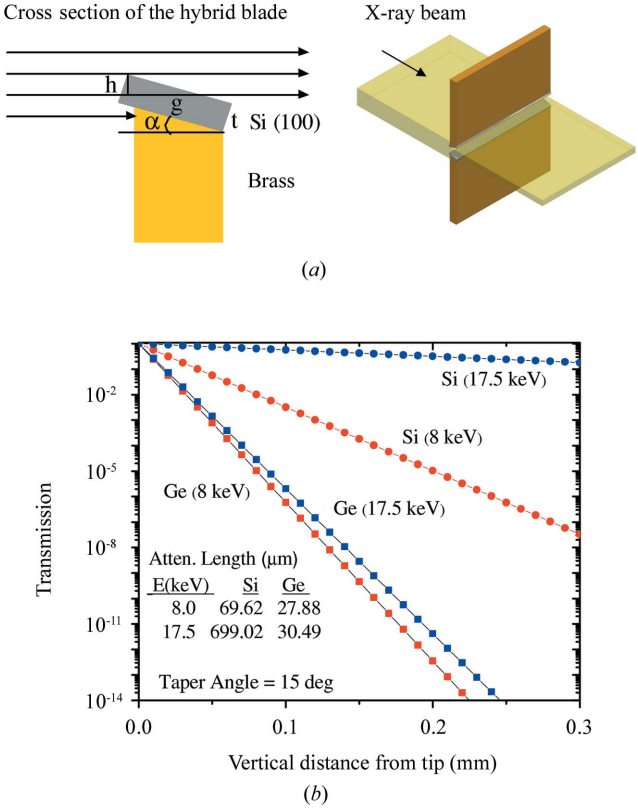

Figure 1
Basic design of the hybrid metal–single-crystal X-ray slit. (*a*) Cross sectional and isometric views of the Si–brass hybrid slit, showing interaction with X-rays. (*b*) Calculated transmission through the tip region for Si- and Ge-edged slits for 8 and 17.5 keV X-rays to simulate performance for Cu $K\alpha$ and Mo $K\alpha$ radiation, respectively (the attenuation lengths are listed in the graph).

The tapered design is crucial to achieving the scatterless performance of the hybrid slit. The tapering angle α, which is selected to be much larger than the incident beam divergence, prevents any possibility of grazing incidence of the X-ray beam on the top and side surfaces of the Si strip, which would otherwise produce specular and diffuse scattering that may be even more intense than the slit scattering from metal slits (Gehrke *et al.*, 1995; Als-Nielsen & McMorrow, 2001). In this large-tilt regime, the beam is defined only by the edge where the top and side surfaces of the Si substrate meet, which is extremely sharp in general and therefore produces very little scattering. We have found that no special edge polishing is required to achieve scatterless performance. The importance of using a large tapering angle was confirmed by experiments with Si hybrid slits that were tapered by 5, 20 and 35.5°. The 5° tapered slits still generated slit scattering, albeit at a much lower level in comparison with the metal slits. In contrast, the hybrid slits with 20 and 35.5° angles produced no observable slit scattering at all.

As shown in Fig. 1(*a*), near the tip of the slit the Si thickness is finite and some X-ray transmission through the tip is inevitable, with the undesirable effect of decreasing the sharpness of the beam profile. The tip attenuation function is dependent on the taper angle, the material density and the X-ray energy. The effective thickness, g, increases away from the tip, as determined by

$$g = h/\sin\alpha\cos\alpha = 2h/\sin(2\alpha), \qquad (1)$$

where h is the vertical distance from the tip and α is the taper angle. Equation (1) holds true for $h < h_{\max} = t\cos\alpha$, where t is the thickness of the substrate. Beyond $h_{\max}$, the effective thickness $g_{\max} = t/\sin\alpha$ is constant. It is clear from equation (1) that a smaller tapering angle would lead to less transmission through the tip. However, in order to eliminate surface scattering, a larger taper angle is preferred to prevent any X-rays from impinging on the top surface of the substrate. Balancing these two opposing requirements, we surmise a tapering angle of 10–20° would suffice for most SAXS instruments.

The choice of material for the single-crystal tip has a much larger effect on X-ray transmission than the taper angle. The X-ray transmission through the tip as calculated from equation (1) is shown in Fig. 1(*b*) for Si- and Ge-edged slits with a 15° taper angle for 8 and 17.5 keV X-rays (Cu K_α and Mo K_α radiation). The data show that the Ge slit provides orders of magnitude better attenuation than Si at both energies. However, as validated by our results, Si-edged slits are adequate for most applications with a laboratory Cu target X-ray source, with only 1% transmission 80 μm from the tip. In addition to Si and Ge, there are many other high-quality single-crystal substrates that are commercially available. Standard semiconductor wafer substrates are attractive

because of the fact that they are all near-perfect single crystals (hence no scattering from defects), are readily available at reasonable cost, and can be ordered in custom sizes. Based on comparison of the energy-dependent attenuation lengths of Si, Ge, GaAs, GaSb, InP and InAs, we found that InP actually offers the best attenuation at energies < 12 keV, while Ge is a better choice above 12 keV. The large attenuation factors for Ge- and InP-based slits indicate that they are excellent choices for synchrotron-based SAXS instruments. For higher-energy applications, other higher-density materials such as single-crystalline tungsten may be considered.

As indicated by equation (1), the thickness of the single-crystal substrate has no effect on attenuation in the immediate vicinity of the tip. However, it does determine the maximum attenuation factor that can be achieved. The calculation shown above suggests that, with a high-density slit edge (*e.g.* Ge), there is very little advantage to using a substrate that is thicker than the commonly available 0.5 mm wafer material, even at synchrotron flux levels.

3. Hybrid slits-based single-aperture SAXS camera

The performance of the Si-edged hybrid slits was characterized on a custom-built SAXS instrument consisting of a 50 W microfocus (source size ~50 µm) sealed-tube X-ray generator combined with a parallel-beam multilayer monochromator (GENIX from XENOCS), three motorized *x*–*y* slits (only one was used, see text below), an evacuated X-ray beam path and a Bruker HI-STAR multiwire area detector (1024 × 1024 image size with 100 µm pixels). The sample-to-detector distance was 1740 mm. The instrument was constructed with polished tungsten slits with a 35.5° tapered edge. To convert the system to the hybrid slits, (100)-oriented Si strip substrates (2.5 × 30 × 0.5 mm) were bonded directly onto the tapered edge of the existing tungsten blades.

The use of the scatterless hybrid slits enabled us to simplify the design of the SAXS instrument to using, theoretically, just

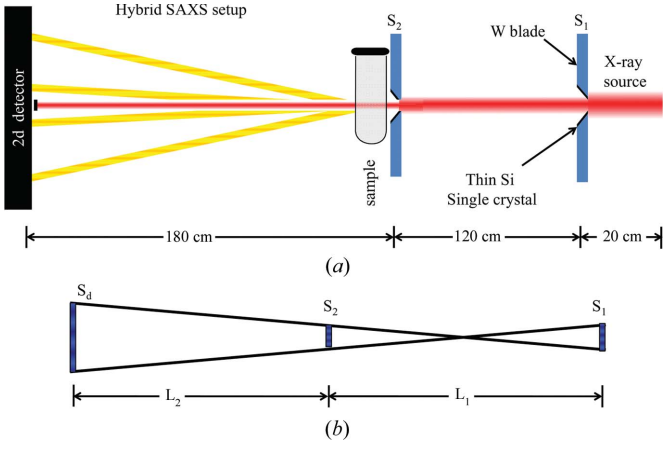

Figure 2
Optical configuration of SAXS diffractometers. (*a*) Schematic diagram of the hybrid slit-equipped SAXS instrument used in the experiments. (*b*) Simplified geometric ray-tracing model of the two-aperture SAXS setup. For the current work, the first slit was kept outside the beam. Thus, the instrument is effectively a single-slit SAXS camera.

two sets of *x*–*y* slit, as shown schematically in Fig. 2(*a*). Currently, the prevalent two-dimensional SAXS design uses three pinholes (slits) to achieve the required low-angle access (Pedersen, 1993); the first two pinholes are used to set the beam collimation, while the third one (guard slit) is used to limit the cone of slit scattering. Since no slit scattering is produced from the hybrid slit, the third (guard) slit is no longer needed.

Further investigation led to the realization that even the first slit is not required under the right conditions, and we refer to this much simplified design as a single-aperture SAXS camera. Effectively, for most instruments, the primary beam monochromator, which typically produces a low-divergence beam with a well defined size, can act as the first slit. We can derive the design principle by first considering a typical two-aperture SAXS setup, which is represented in the geometric ray-tracing model in Fig. 2(*b*). Optically, one may simply consider the SAXS instrument as a large pinhole camera, in which the defining aperture (S_2) projects the effective source (S_1, defined by either an incident aperture or the monochromator) directly onto the detector. Regardless of the incident beam divergence or the type of slit used for S_1, and as long as the defining aperture S_2 is scatterless, the maximum beam size on the detector plane can be calculated using simple geometry (Riekel *et al.*, 2000; Shaffer & Hendricks, 1974):

$$S_d = S_2 + (S_1 + S_2)L_2/L_1 = S_2 + 2\delta L_2, \qquad (2)$$

where $\delta = (S_1 + S_2)/2L_1$ is the aperture-defined maximum beam divergence. Assuming that the sample is placed very close to S_2, one can then take L_2 as the sample-to-detector distance and calculate the resolution of the SAXS instrument:

$$q_{min} = \pi S_d/\lambda L_2. \qquad (3)$$

For two-dimensional SAXS with a symmetric beam, realistically the right-hand side of equation (3) should be multiplied by $2^{1/2}$ to account for the fact that the maximum beam dimension for the typical square beam shape should be measured diagonally. Based on equation (3), it is possible to adjust the defining aperture size S_2 and the distances L_1 and L_2 so that S_1 matches the actual beam size at the monochromator. This can essentially eliminate the need for the S_1 slit altogether, leading to a SAXS setup with just one aperture. This new design concept was implemented and validated on the in-house instrument shown in Fig. 2(*a*), by moving S_1 completely outside the beam and using S_2 as the sole defining aperture in the system (the beam size at the exit of the monochromator was 1.2 × 1.2 mm).

The substantial reduction of the number of apertures in the instrument (from three to one) resulted not only in a much simpler optical configuration, but more importantly in a dramatic increase of usable X-ray flux on the sample as well. Experimentally, a threefold flux increase was observed compared with the three-slit setup, without changing the distances between slits, resulting in a total flux of ~3.2 × 10^7 photons s^{-1} on a 0.8 × 0.8 mm spot at the sample position with the X-ray source operating at 48 kV × 1 mA (48 W). It is

likely that further flux enhancement is possible by design optimization. It is important to point out that this high-flux single-aperture SAXS camera design does not compromise the resolution of the SAXS performance at all, owing to the use of the scatterless slits, as demonstrated below. In fact, because of the lower scattering background, we were able to achieve a lower $q_{\min}$ (from 0.01 to 0.0075 Å^{-1}) on the same setup without changing any other components.

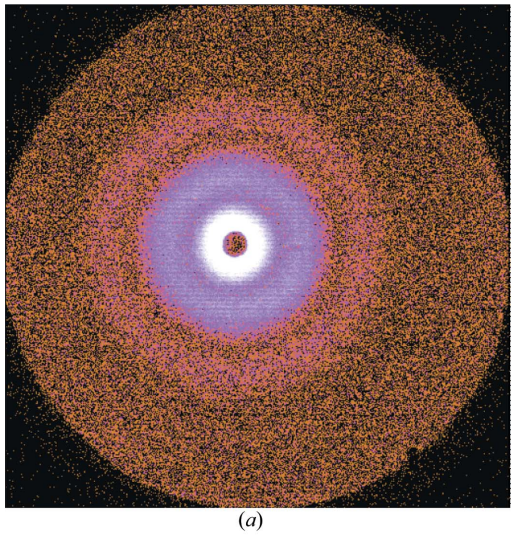

(*a*)

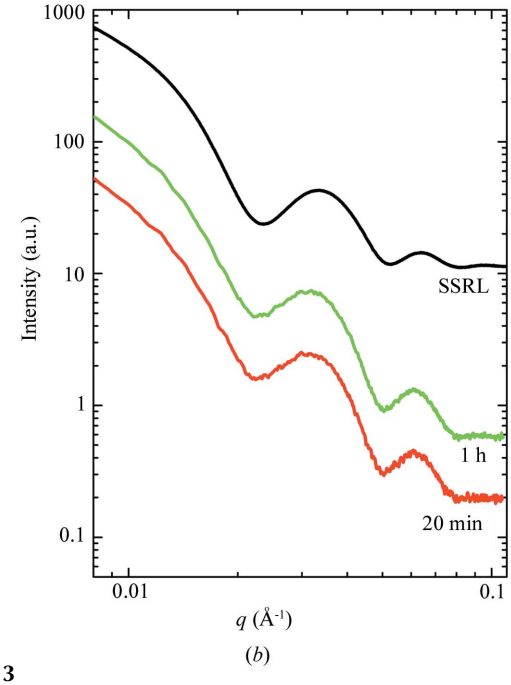

(*b*)

Figure 3
Diffraction data collected on the single-aperture SAXS instrument. (*a*) Two-dimensional SAXS data (20 min exposure) from bovine microtubules in solution measured with the in-house 50 W X-ray microfocus source. (*b*) Azimuthally averaged diffraction intensity *versus* wavevector q, showing the cylindrical form-factor peaks of microtubules. Data processing was carried out using the *FIT2D* program developed at ESRF (Hammersley, 1997). Red and green lines show data for 20 and 60 min exposures, respectively, whereas the black line shows data measured on a similar sample at SSRL for 10 min. The structure details are well represented even at 20 min exposure, largely because of the threefold intensity enhancement from the single-aperture SAXS setup.

4. Results and discussion

To demonstrate the performance of the new single-aperture SAXS instrument, we show in Fig. 3 two-dimensional X-ray diffraction data measured in-house from a solution sample of microtubules (MT) suspended in buffer (MT concentration 4.24 mg ml^{-1}, total amount of bovine tubulin in the sample = 150 µg) in a 1.5 mm quartz capillary (Raviv *et al.*, 2005). The form-factor rings from the hollow 25 nm-diameter microtubules are visible on the detector within seconds of exposure and are quite well developed after a 20 min exposure (Fig. 3*a*). In Fig. 3(*b*), the azimuthally averaged scattering data $I(q)$ are compared with the 10 min exposure data collected at SAXS beamline 4-2 at Stanford Synchrotron Radiation Laboratory (SSRL) on a sample with the same MT concentration. Although the intensity of the data collected in-house is much lower, the relevant features are all well defined, a remarkable feat given that only a 50 W X-ray source was used.

To compare quantitatively the performance of conventional tungsten and hybrid Si slits, we scanned a single blade of both types of slit across the X-ray beam at the sample position and recorded the slit scattering pattern with a two-dimensional detector. In Fig. 4, we show a series of two-dimensional slit

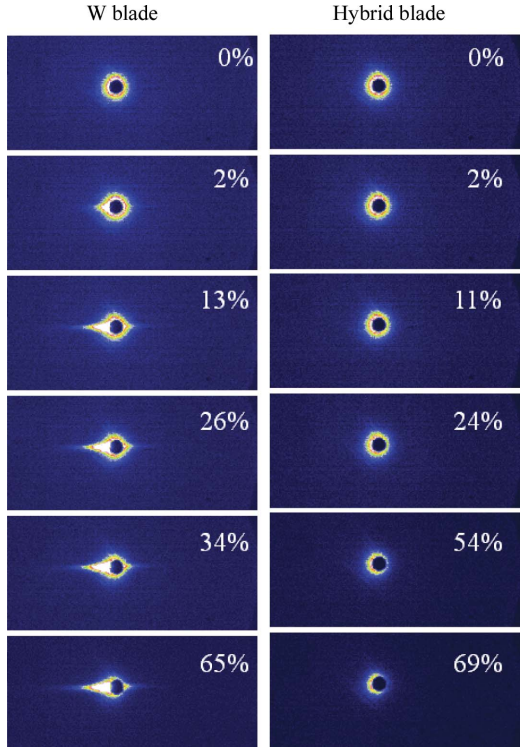

Figure 4
Two-dimensional SAXS data recorded as tungsten (left-hand panel) and hybrid (right-hand panel) slit blades were moved into the main beam from right to left, as indicated by dimming of the background on the right-hand side of the image. Percentages indicate the relative reduction from maximum intensity as normalized from PIN diode detector measurements of the direct beam intensity after the blade. While slit scattering is visible for the tungsten blade as soon as it touches the beam at 2% reduction, the hybrid blade produces no visible slit scattering at all while cutting up to two-thirds into the main beam.

scattering patterns as the blades were driven across the beam horizontally from right to left. The percentage marked in each image represents the relative beam intensity (as measured by a PIN diode detector) loss due to the blade cutting into the beam, with 0% corresponding to the blade being positioned completely outside the beam. On the left-hand panel, strong low-angle slit scattering is clearly observed as the tungsten blade cuts into the X-ray beam (the slit scattering is evident even at 2% blockage, becoming more intense with increasing beam blockage). In comparison, as shown in the images on the right, the Si-tipped hybrid blade produces no observable slit scattering at all as it cuts into the main beam, as evidenced by the gradual dimming of the diffraction images from top to bottom, where it is blocking two-thirds of the beam intensity.

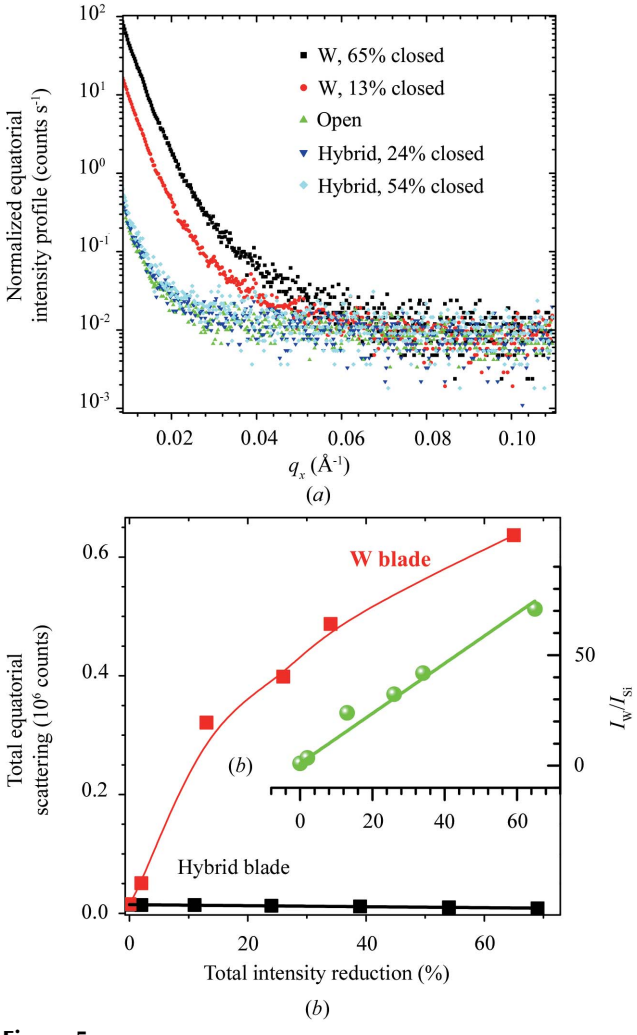

Figure 5
Slit scattering data from tungsten and hybrid slit blades. (*a*) Normalized scattering intensity profile along the slit scattering direction for tungsten and hybrid blades at different levels of beam cutting. The data are produced by a line scan from the beam center towards the left in the raw diffraction images shown in Fig. 4. The intensity at each point of the profile represents the total counts over the width of the line, which was set to 11 pixels, corresponding to a 1.1 mm vertical beam size on the detector. Data have been normalized with the open beam intensity when the slit blade was outside the beam in order to put all curves on the same scale. (*b*) Integrated equatorial slit scattering (sum of all counts) over the full q range as a function of beam intensity reduction, without intensity re-normalization. (Inset) Ratio of total scattering from a conventional tungsten slit blade to that from an Si-tipped hybrid blade, indicating that the performance gain using the scatterless slit increases with the flux level at the position of the blade.

The slit scattering, whenever present, dominates the small-angle scattering signal. In Fig. 5(*a*), we show SAXS intensity profiles extracted from images shown in Fig. 4 along the equator line where the slit scattering is most prominent (from beam center to the left in the scattering images). In order to compare the slit scattering more quantitatively, the data were normalized to the total intensity (as measured by a PIN diode detector) of the first image when the slits were outside the beam. As expected, the slit scattering is most intense in the low-angle region ($q < 0.03$ Å^{-1}), where the tungsten blade produces close to two orders of magnitude higher background scattering. This underscores the well known fact that slit scattering is the main limiting factor of resolution in conventional SAXS instruments. For the hybrid blade, the normalized small-angle scattering remains essentially the same, regardless of how much the blade cuts into the beam, confirming that the slit produces no observable slit scattering at all. Furthermore, no increase in the scattering at larger angles between $0.08 < q < 0.12$ Å^{-1} is observed as the hybrid blade cuts into the beam. Additional experiments extending up to $q \simeq 3.1$ Å^{-1} ($2\theta \simeq 45°$) confirmed that the slits produce no extraneous scattering even in the wide-angle regime.

The divergent low-angle scattering behaviour of the hybrid Si and conventional tungsten slit blades is even more dramatic, as shown in Fig. 5(*b*), when comparing the integrated intensity along the equator (a measure of total slit scattering) as a function of beam attenuation. For the hybrid blade we find that the total slit scattering decreases slowly as the beam is cut. This can be explained by reduced overall parasitic scattering other than slit scattering, *i.e.* from air and the Kapton window in the X-ray path, both of which scale with the incident beam intensity. It is only because of the scatterless nature of the Si slit that this secondary effect becomes clearly observable. In contrast, for the tungsten blade, the total equatorial intensity actually increases as a direct result of increased slit scattering, owing to the fact the blade is exposed to the more intense central part of the beam as it cuts through the beam (similar to an inverted knife-edge scan). Therefore, one could take the ratio of the overall slit scattering intensity for the two types of slits as a reasonable quantitative measure of performance gain, as shown in the inset in Fig. 5(*b*), where a maximum gain of about a factor of 75 was achieved by using the scatterless Si slit. More importantly, one arrives at a significant realization that this gain actually increases with the incident beam intensity, which means that the use of scatterless slits is more necessary for synchrotron-based SAXS instruments where they could yield even higher performance enhancements.

In addition to having clear advantages for SAXS, hybrid scatterless slits can potentially be used for beam conditioning in other X-ray diffraction techniques in which a sharper beam profile can reduce peak separation, leading to better data quality. This is important, for example, for high-resolution X-ray diffraction from semiconductor thin films and super-

lattice heterostructures which generate closely spaced fringe peaks, and similarly in large unit cell macromolecular crystallography (*e.g.* for protein complexes and viruses).

Although the experimental results presented above were obtained from an in-house SAXS diffractometer, the hybrid slit can also be used in synchrotron-based SAXS instrumentation. It is possible that, for synchrotron applications where the flux level is many orders of magnitude higher, other secondary scattering effects, such as diffuse scattering due to phonon correlations in the single-crystalline material (Wu *et al.*, 1999), may manifest to a measurable level, thus degrading performance. However, these effects would pale in comparison with slit scattering from conventional metal blades, making the hybrid slit still a more preferable choice. Recent preliminary experiments conducted on the Advanced Light Source (ALS) SAXS beamline 7.3.3 have confirmed that the hybrid design presented here indeed produces no observable slit scattering even at third-generation synchrotron flux levels.

5. Conclusion

We have presented a simple hybrid metal–single-crystal scatterless slit design that can be used to improve dramatically the performance of both in-house and synchrotron-based SAXS and other high-resolution X-ray diffraction instrumentation. Experimental results show that the hybrid slit produces no observable slit scattering, leading to a much simplified single-aperture optical design for SAXS with dramatically increased intensity and improved low-angle data quality. Although this paper has focused on slit apertures, the same design principle can be applied to fabricate scatterless pinholes as well. Because of its simplicity this design can be readily adopted to retrofit current SAXS diffractometers for enhanced performance.

This work was supported by an NSF MRI (Major Research Instrumentation) Development Grant (No. DMR-0619171). The authors thank C. R. Safinya and S. Sinha for insightful discussions, and L. Wilson and H. Miller for providing the tubulin material. We thank E. Gann and A. Hexamer at the Advanced Light Source (ALS) for help with synchrotron-based experiments. RB acknowledges fellowship support from the Human Frontier Science Program organization and TH acknowledges support from the RISE program at UCSB Materials Research Laboratory, which is supported by the MRSEC Program of the National Science Foundation under award No. DMR-0520415.

References

Als-Nielsen, J. & McMorrow, D. (2001). *Elements of Modern X-ray Physics*, ch. 3. New York: J. Wiley and Sons Inc.
Bösecke, P. & Diat, O. (1997). *J. Appl. Cryst.* **30**, 867–871.
Gehrke, R, Bark, M., Lewin, D. & Cunis, S. (1995). *Rev. Sci. Instrum.* **66**, 1354–1356.
Hammersley, A. P. (1997). *FIT2D*. ESRF, Grenoble, France.
Pedersen, J. S. (1993). *Modern Aspects of Small-Angle Scattering*, NATO ASI Series, edited by H. Brumberger. Dordrecht: Kluwer Academic Publishers.
Raviv, U., Needleman, D. J., Li, Y., Miller, H. P., Wilson, L. & Safinya, C. R. (2005). *Proc. Natl Acad. Sci. USA*, **102**, 11167–11172.
Riekel, C., Burghammer, M. & Müller, M. (2000). *J. Appl. Cryst.* **33**, 421–423.
Shaffer, L. B. & Hendricks, R. W. (1974). *J. Appl. Cryst.* **7**, 154–158.
Sinha, S. K., Sirota, E. B. & Garoff, S. (1988). *Phys. Rev. B*, **38**, 2297–2311.
Wu, Z., Hong, H., Aburano, R., Zschack, P., Jemian, P., Tischler, J., Chen, H., Luh, D.-A. & Chiang, T.-C. (1999). *Phys. Rev. B*, **59**, 3283–3286.
Zemb, T., Taché, O., Né, F. & Spalla, O. (2003). *Rev. Sci. Instrum.* **74**, 2456–2462.